sustainability

MDPI

Article

Enhancing the Performance of Human Motion Energy Harvesting through Optimal Smoothing Capacity in the Rectifier

Ilgvars Gorņevs * and Juris Blūms

Institute of Technical Physics, Faculty of Materials Science and Applied Chemistry, Riga Technical University, LV-1048 Riga, Latvia; juris.blums@rtu.lv

* Correspondence: ilgvars.gornevs@inbox.lv

Abstract: Energy harvesting offers a promising solution for powering a growing variety of low-power electronics; however, harnessing energy from human motion, with its irregular and low-frequency bursts of power, presents conversion challenges. As rectification is a common part of it, this study investigates the influence of smoothing capacitor values on rectifier output for short, intermittent signals. We propose an analytical model that identifies an optimal smoothing capacity for the full-bridge rectifier, considering harvester internal resistance, frequency, and load resistance and leading to the highest average output voltage after rectification. The model was validated with detailed computer simulations; furthermore, a similar effect was revealed on a voltage multiplier circuit as well. Experimental measurements demonstrate that deviating from the optimal smoothing capacity results in up to 10% decrease in rectified RMS voltage, leading to significant drops in output power in specific energy harvesting systems. A real-world experiment with a human motion energy harvester further confirmed the findings in a naturally varying generation environment.

Keywords: energy harvesting; circuit optimization; AC/DC; rectifiers; voltage multipliers

Citation: Gorņevs, I.; Blūms, J. Enhancing the Performance of Human Motion Energy Harvesting through Optimal Smoothing Capacity in the Rectifier. *Sustainability* **2023**, *15*, 13564. https://doi.org/10.3390/su151813564

Academic Editors: Erol Kurt and Jose Manuel Lopez-Guede

Received: 9 August 2023
Revised: 2 September 2023
Accepted: 9 September 2023
Published: 11 September 2023

1. Introduction

Portable electronics have demonstrated an ongoing increase in efficiency and decrease in size, allowing them to experience a remarkable surge in popularity. Particularly, the Internet of Things (IoT) is becoming widespread and has a potential to revolutionize various aspects of our daily lives, providing previously unavailable health and safety information [1–4]. However, the effective utilization of IoT devices is heavily dependent on their power source, as the increasing demands for performance tend to outrun the development of battery technologies [5]. Need for frequent recharging or replacing puts a significant limitation on the creation of convenient monitoring devices that can be either placed in hard-to-reach places or integrated into everyday accessories. Energy harvesting can be seen as a potential solution to alleviate the reliance on external power supplies or even eliminate it altogether in the most optimal scenario. It has been shown that by harnessing energy from the environment, such as mechanical vibrations [6] or solar radiation [7], IoT can be powered in various degrees of success.

Energy harvesting, particularly when utilizing human activity as the input source, has been a subject of extensive investigation in the scientific community. Numerous articles have delved into enhancing materials [8,9] and refining methods [10,11] to maximize energy capture. Additionally, there has been a focus on creating self-sustaining energy sources tailored for low-power electronics [12–14]. Despite the considerable attention, only a limited number of studies have addressed the details of energy conversion and its efficiency [15–17]. Such oversight may limit our understanding of the overall viability and performance of these harvesting systems.

An important aspect of energy harvesters lies in their distinct voltage generation characteristics. Some harvesters are capable of producing a sufficient voltage level [18,19], rendering them potentially suitable for direct usage by low-voltage electronics, while other types of energy harvesters require voltage boosting to reach the required levels [16,17]. Moreover, motion-based energy harvesters often require rectification to convert the harvested energy into usable DC power. Unfortunately, this process can introduce significant losses, which are highly dependent on the load value [15]. To mitigate such losses, researchers have explored various approaches, such as employing lower forward-voltage drop elements [20] or utilizing active rectifiers [21]. At the same time, the impact of the rectifier's smoothing capacity is often neglected, yet it plays a pivotal role in maintaining a stable DC output.

The smoothing filter capacity after the rectifier elements is an essential stage in the conversion of AC to DC, as without it, there would be only separate voltage pulses with a drop to zero between them, which is rarely satisfactory. Efforts to analyze this important step are not new; they began with a graphical analysis of the vacuum tube diode both ignoring and taking into account resistive losses in the circuit before the filter elements [22]. Many studies simplify the analytical model by considering only the load resistance in the circuit, ignoring the other losses [23–25], while others propose a symbolic solution in lossy systems [26,27]. Rectifier elements are commonly represented as ideal switches to simplify the analysis. However, for a more comprehensive examination of their behavior, additional parameters such as the voltage drop or equivalent resistance can be incorporated [22]. By considering these parameters, a detailed analysis of characteristics including peak, average, or root-mean-square (RMS) current can be conducted. In the context of a full-wave rectifier circuit, where considerations include losses apart from the load, it is observed that increasing the smoothing capacity leads to a reduction in rectified voltage ripple (the difference between the highest and lowest voltage levels) and an increase in the mean value. However, the presence of losses imposes limitations on how high the rectified voltage can be relative to the input signal. These losses can originate from various sources but mainly are conduction losses in the diodes and resistive losses in the energy harvesters themselves, as the latter can exhibit relatively high internal resistance [14,28].

Existing models put emphasis on a steady state in the system, which is achieved with a long, periodic, and constant signal at the input. That means harvesters with a stable generated signal can theoretically benefit from increasing the smoothing capacity until the desired stability of the rectified signal is achieved. However, a long and stable signal can be a seldom the case with sporadic nature of energy harvesting. Human motion energy harvesters, mainly those working without mechanical resonance, generate irregular and relatively short bursts of power due to the slow motion speed at a low frequency [18,19,29–31], and this state lies beyond the scope of the models mentioned. Therefore, the main objective of this study was to investigate the influence of the smoothing capacitor value on a rectifier's output when dealing with circuits with additional losses and intermittent input signals. Two rectification schemes were investigated: a full-bridge rectifier, for which an analytical model was proposed, and a voltage doubler, which was simulated using computer models. The rest of the paper is structured as follows. Section 2 outlines the proposed analytical model for the full-bridge rectifier. In Section 3, the model's validity is confirmed by comparing its results with detailed computer simulations (Section 3.1). Subsequently, experimental measurements were conducted using a signal generator and a switching load for both the full-bridge and voltage-doubler circuits at a range of smoothing capacities (Section 3.2). Section 3 concludes with experimental measurements of the voltage doubler utilizing a human motion energy harvester and a low-voltage converter, testing the predefined influence of the used capacity values in a naturally varying environment (Section 3.3). In Section 4, strengths and limitations of the model are reviewed, including a comparison with existing stationary input signal model for the full-bridge rectifier, followed by a discussion of the overall results and their implications. Lastly, Section 5 presents brief conclusions derived from the findings presented in the article.

2. Materials and Methods

One of the most straightforward methods to assess the impact of circuit parameters is by using most of SPICE–based circuit simulation programs. These programs offer the flexibility to set a wide range of parameters, enabling the evaluation of actual schematics with desired level of details, for instance, by incorporating non-linear rectifier elements with realistic current–voltage (I–V) curves provided by manufacturers and including pre-recorded harvester signals (Figure 1a) as inputs. Although transient signal analysis using these simulation programs allows for extensive testing and the attainment of highly precise results, it can be computationally demanding and rather time-consuming. Therefore, an analytical model is proposed in this study to alleviate these challenges for a full-bridge rectifier.

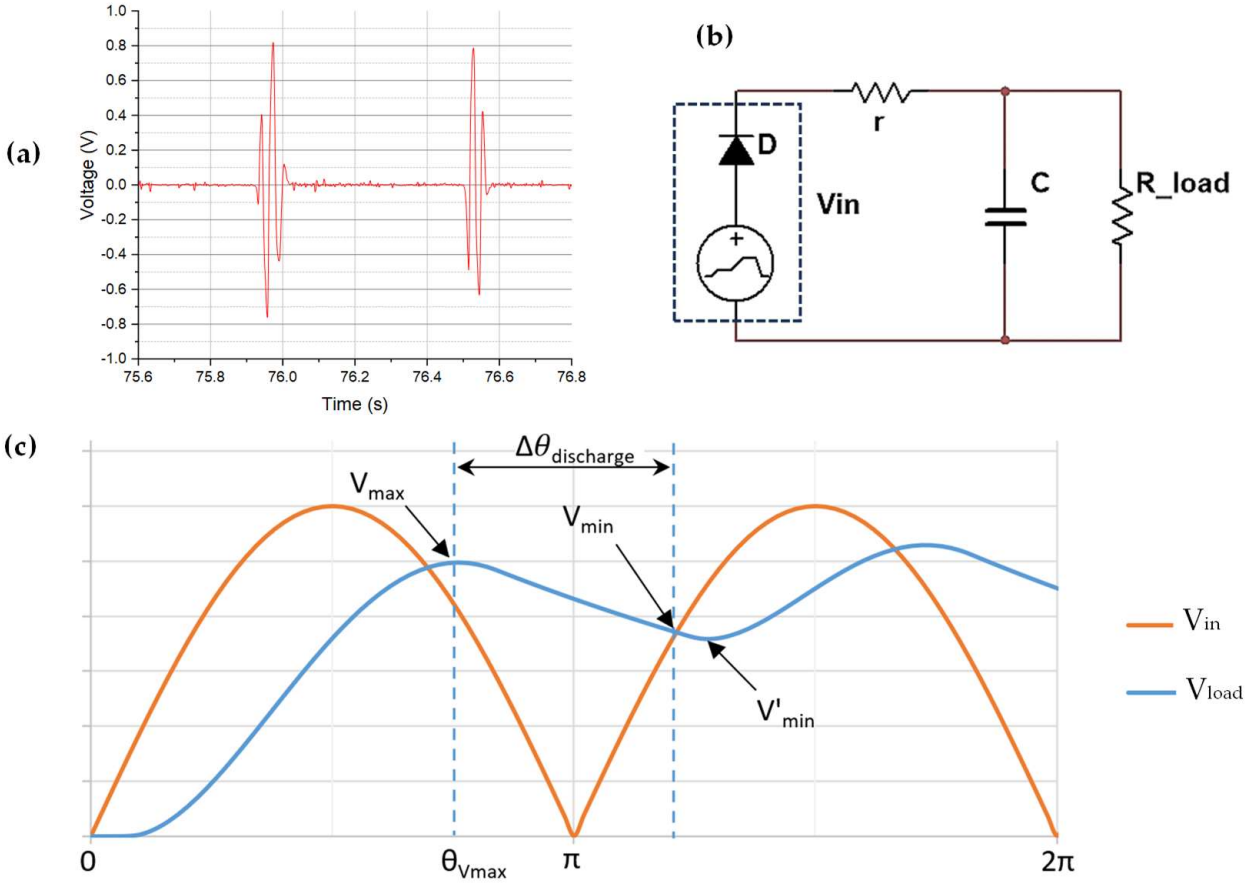

Figure 1. Typical generated signal of the harvester presented in [31] (**a**); proposed model circuit (**b**); the analyzed voltage characteristics (**c**), where V_{in}, input signal as $|Sin(\theta)|$; V_{load}, realistic output voltage; V_{max}, highest output voltage between first two input pulses; $\Delta\theta_{discharge}$, assumed capacitor discharge region; V_{min}, assumed minimal output voltage between two input pulses; V'_{min}, actual minimal output voltage between two input pulses.

The circuit of the model consists of an ideal source V_{in} producing the modulus of a sine wave, a resistor r encapsulating all losses, a smoothing capacitor C, and the load resistance R_{load} (Figure 1b). It is assumed that the current cannot flow back into the source; thus, this setup emulates rectification of the both periods of the sine wave with ideal switches, where the losses like internal resistance of the generator or the switches are constant (r). To construct the model, several assumptions were made (Figure 1c):

- The charging voltage starts from 0 and reaches V_{max}, determined by the characteristics of the input signal, C, r, and R_{load};

- The discharging starts after reaching peak voltage V_{max} at θ_{Vmax}, but due to the delay induced by the resistance and capacitance, θ_{Vmax} is offset from the input signal peak occurring at $\pi/2$;
- Discharging stops when the rising edge of the second pulse of the source voltage V_{in} matches the discharging voltage (V_{min}).

The model aims to describe the voltage change between the first two pulses and, consequently, forecast V_{max} and V_{min}. To simplify matters, the absolute values of these voltage values are not deemed critical but rather their dependance on various combinations of C, r, R, and input signals. As a result, we neglect the fact that the discharge actually begins later at a voltage lower than the maximum value, V_{max}, because initially load voltage tracks the descending input signal while the rectifier diodes are still open due to minimal voltage difference. Similarly, the discharge terminates slightly later at V'_{min}, as it is shown on the picture (Figure 1c), and consequently, these assumptions partially cancel each other.

The highest reachable voltage can be estimated from a voltage divider Equation (1), where X_c, the reactance of the capacitor C (2), is in parallel to load R_{load}. By calculating the magnitude of the resulting impedance value, Equation (3) can be obtained, where f is the frequency of the input signal.

$$\frac{R_{load}||X_C}{R_{load}||X_C + r} \cdot V_{in} \tag{1}$$

$$X_C = \frac{1}{2\pi f C} \tag{2}$$

$$V_{max} = \frac{R_{load} \cdot V_{in}}{\sqrt{(r + R_{load})^2 + (2\pi f C r R_{load})^2}} \tag{3}$$

The discharge voltage can be mathematically characterized as a function of phase angle θ by Equation (4), where θ_{Vmax} is the moment when the maximal voltage is reached and the discharge is assumed to begin. In the case of a simple RC series circuit, the capacitor reaches its highest voltage when the source current drops to zero. However, this occurrence does not coincide with the moment when the voltage reaches zero (as depicted in Figure 1c, V_{in} at π); therefore, the offset between the current and the source voltage needs to be determined using Equation (5). To obtain a series connection, the Thevenin equivalent is used, assuming the capacitor C is initially the output (Figure 2). The resulting equivalent circuit, which incorporates a single equivalent resistor encompassing both losses r and the load R_{load}, is well suited for the analysis, as the current dropping to zero and changing directions will mean the discharge of the capacitor C has started. The estimation of the equivalent resistance can be accomplished using Equation (6), while the magnitude of the equivalent source can be determined by Equation (7); however, magnitude is insignificant for the delay calculations and thus is disregarded.

$$V_{discharge} = V_{max} \cdot e^{-\frac{\theta - \theta_{Vmax}}{2\pi f C R_{load}}} \tag{4}$$

$$\Delta\theta_{current} = -ArcTan\left(\frac{X_c}{R}\right) \tag{5}$$

$$R_{eq} = \frac{r \cdot R_{load}}{r + R_{load}} \tag{6}$$

$$V_{eq} = V_{in} \cdot \frac{R_{load}}{r + R_{load}} \tag{7}$$

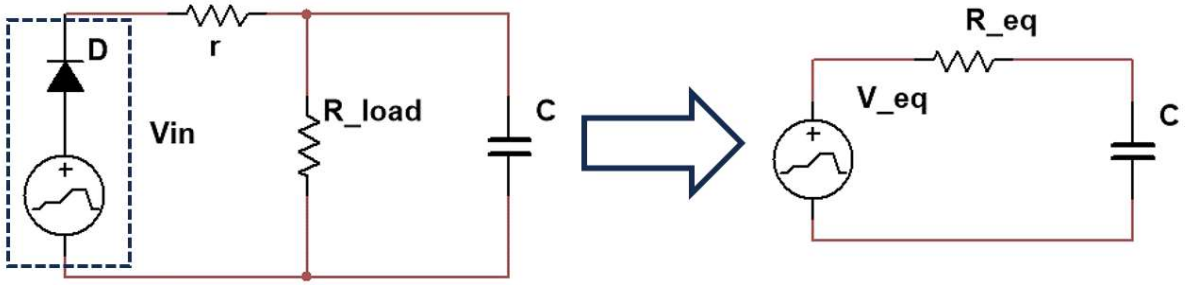

Figure 2. Creating an equivalent series circuit.

Through the utilization of equivalent resistance (6) in the determination of the current offset (5) and the following combination of the resulting equation with Equations (3) and (4), we derive Equation (8). Notably, it is evident that V_{in} solely influences the scale factor and can be substituted with 100 in both Equations (3) and (8) to obtain the results as a percentage relative to the input signal. Equation (8) describes the discharge process between the first and second input voltage pulses, and in order to attain V_{min}, the conditions stated in Equation (9) must be satisfied, as depicted in Figure 1c for $\Delta\theta_{discharge}$.

$$\begin{aligned} V_{discharge} &= \frac{V_{in}\ R_{load}}{\sqrt{(r+R_{load})^2+(2\pi f\ C\ r\ R_{load})^2}} \cdot e^{-\frac{\theta-(\pi-ArcTan[\frac{1}{(2\pi fCReq\ )}])}{2\pi fCR_{load}}} \\ &= \frac{100\ R_{load}}{\sqrt{(r+R_{load})^2+(2\pi f\ C\ r\ R_{load})^2}} \cdot e^{-\frac{\theta-\pi+ArcTan[\frac{r+R_{load}}{2\pi f\ C\ r\ R_{load}}]}{2\pi fCR_{load}}} \end{aligned} \quad (8)$$

$$V_{min} = V_{discharge} = V_{in} \text{ for } \pi \leq \theta \leq 1.5\pi \quad (9)$$

The most straightforward approach to solving Equation (9) is through a graphical method. In this method, the known values are the load value R_{load}, losses represented by the internal resistance of the energy harvester r, and the frequency of the generated signal f, which are typically available. This leaves two remaining inputs in Equation (8)—the smoothing capacity C and the present phase angle θ—, resulting in the magnitude $V_{discharge}$; thus, it can be represented using a 3D graph (Figure 3a). The input signal V_{in} does not depend on the smoothing capacity and rather relies on the phase angle (Figure 3b). By plotting the graphs of both the input signal V_{in} and the magnitude $V_{discharge}$ together, as dictated by Equation (9), their intersection represents V_{min} and can be observed on Figure 3c. This graphical representation clearly illustrates that V_{min} exhibits a non-linear relationship with the smoothing capacity, featuring a prominent peak value between the first two input signal pulses just above 500 µF. For more comprehensive evaluation, the intersection can be extracted as a projection and plotted on a 2D graph along with Equation (3) for V_{max} (Figure 3d). The resulting graph shows the dependance of the minimal and maximal voltage values on the smoothing capacity between the first two rectified pulses.

The modeled results reveal that the lowest voltage between the first two rectified pulses initially rises with an increase in the smoothing capacity value, followed by a subsequent decline. In contrast, the highest voltage consistently decreases. This observed trend suggests the presence of an optimal smoothing capacity value, at which the mean rectified voltage reaches its maximum value, indicating the peak performance of the full-bridge circuit.

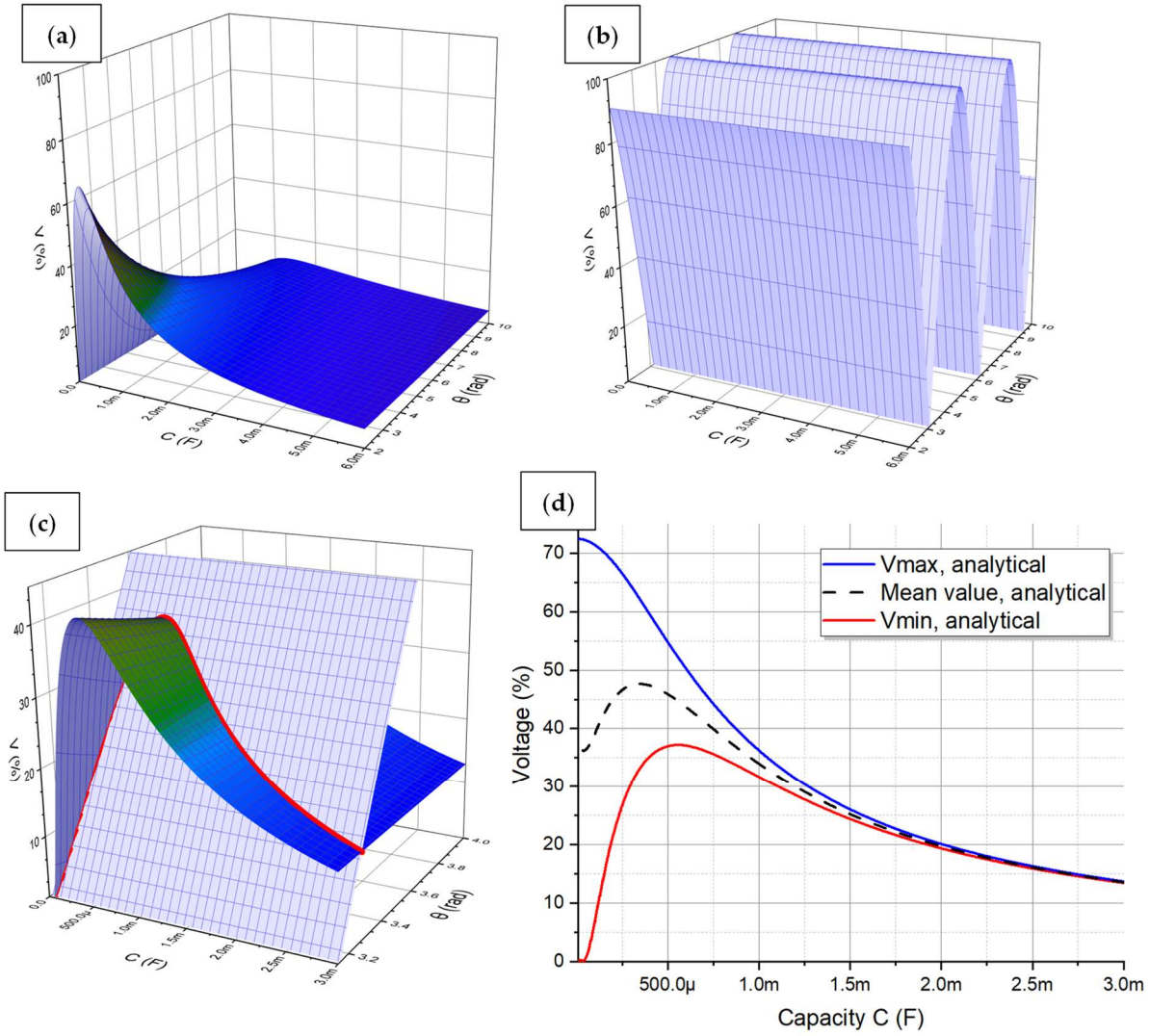

Figure 3. Graphical representation of equations: (**a**) Equation (8); (**b**) input signal as $|Sin(\theta)|$; (**c**) Equation (9), intersection shown with red line; (**d**) extracted intersection (V_{min}) along with Equation (3) (V_{max}) and their mean value. Axis: V, voltage relative to the input; C, smoothing capacity; θ, phase of the signal. Used parameters for the model: R_{load} = 50 Ω; r = 19 Ω; f = 20 Hz.

The proposed model makes an important assumption that the smoothing capacity starts charging from zero. In order for this assumption to hold, it is necessary for the period between the reoccurrence of pulses in the input to be long enough to allow the capacitor to discharge. We assume that the discharge occurs within five time constants of an RC circuit; consequently, the capacity at which the discharge fails to complete can be calculated using Equation (10), where T is the time between repeated input signal pulses in seconds.

$$C_{limit} = \frac{T}{5\ R_{load}} \tag{10}$$

In the case of the input signal used in our study, the pauses between pulses are approximately 0.5 s (as shown in Figure 1a). Considering a load of 50 Ω, the calculated capacity is found to be 2 mF. This value exceeds the predicted peak capacity (Figure 3c), indicating that the modeled results are applicable in this scenario.

3. Results

The current section validates the proposed full-bridge rectifier model through computer simulations, followed by practical experimentation using a signal generator as a source and a switching load, commonly used for low harvested voltage step-up. Additionally, in the study, we examined the impact of capacity on the voltage multiplier circuit, as it enables rectification while utilizing only half the number of diodes required for the full-bridge circuit. An experimental validation using an actual human motion energy harvester was also conducted to evaluate capacity influence predictions under naturally varying signals, thus confirming the robustness of our proposed model.

3.1. Theoretical Validation

To validate the proposed model, it was compared to SPICE-based simulations with various levels of details. Firstly, direct comparison was performed with two input voltage pulses with a circuit, as seen on Figure 1b, and the previously used parameters of R_{load} = 50 Ω, r = 19 Ω, and f = 20 Hz, which resemble an actual energy harvesting circuit example [15]. The simulated highest and lowest voltage (V_{max} and V_{min}) were manually read from the obtained voltage waveforms, while the analytical model results for V_{max} and for V_{min} were added from Figure 3d as a reference. The results show closely matching capacity values for the predicted peaks, which proves the accuracy of the analytical prediction (Figure 4). The relative voltage level is generally higher in the simulated results, with the difference increasing along with higher-capacity values, demonstrating the impact of the basal model assumptions. Nevertheless, the model was not intended to deliver exact voltage values; rather, it is focused on the trend of voltage, which is corresponding.

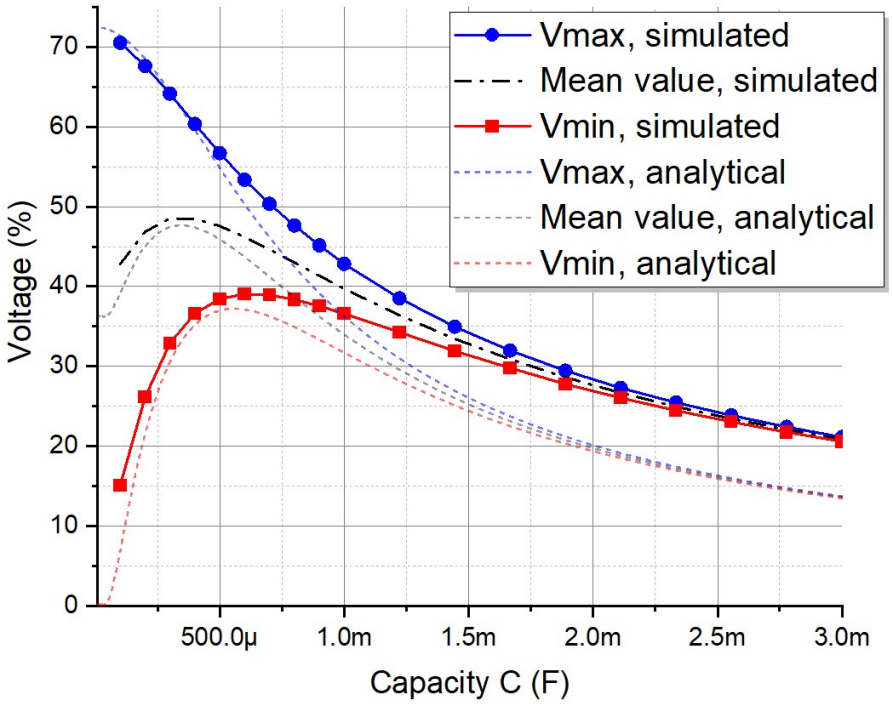

Figure 4. The highest voltage (V_{max}) and the lowest voltage (V_{min}) between the first two rectified signal pulses vs. smoothing capacity value according to the SPICE-based simulation. The proposed analytical model data are taken from Figure 3d. Voltage is shown as a percentage of the input signal amplitude.

To validate the broader impact of the observed relationship effect beyond the highest and lowest voltage peaks between the two pulses, we employed the RMS voltage analysis on the simulated waveform, taking into account the discharge that continued after the

end of the input signal. The RMS values were normalized with respect to the highest attained result, effectively excluding the contribution of the input signal (Figure 5). The results revealed a distinct peak in the capacity range of 400–500 µF. Notably, this peak falls between two peaks predicted by our analytical mode, which is closer to the mean value peak at around 350 µF. The decline of the normalized RMS is notably smaller when offsetting from the peak compared to the model (see Figure 3d, V_{min}). This is attributable to fact that RMS calculation takes into account the whole rectified signal, while the model predicts only the highest and lowest voltage (V_{max} and V_{min}) between the two rectified pulses.

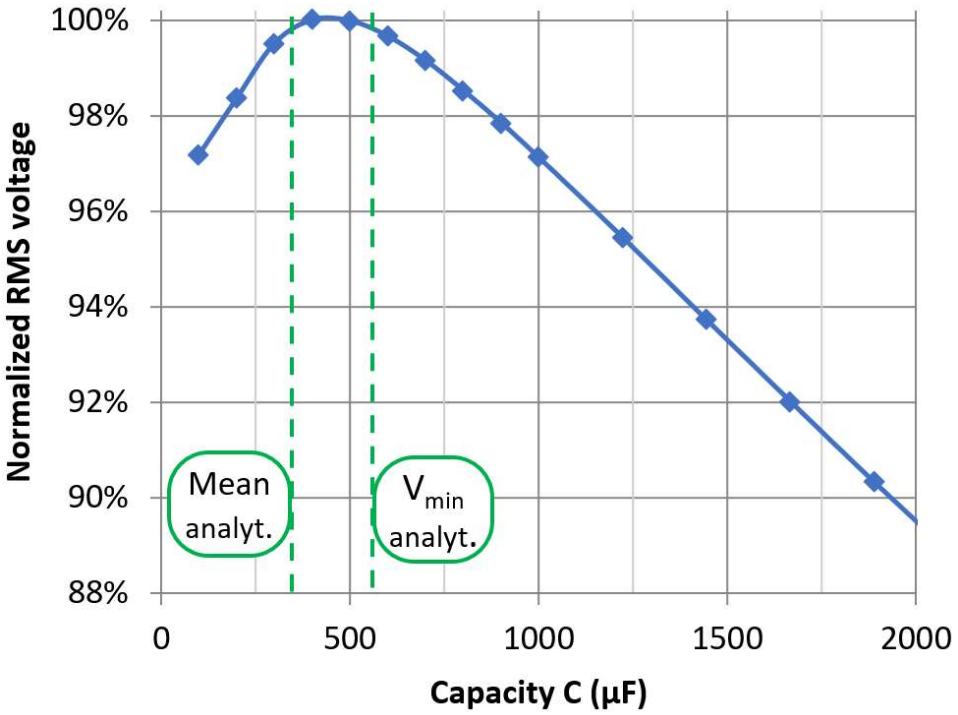

Figure 5. RMS voltage of the whole rectified signal vs. smoothing capacity, calculated from the simulated waveforms including discharge after the two input signal pulses. Green vertical lines represent the capacity values of the mean voltage and the lowest voltage (V_{min}) peaks, as predicted by our analytical model (Figure 3d).

To investigate the impact of non-linear rectification elements, a full-bridge rectifier was implemented using SPICE models provided by the manufacturer for actual diodes [32]. Various input signal lengths were simulated as multiples of sine wave periods: one period produces two rectified pulses, as per the model. Additional losses introduced by these rectifier elements have the effect of shifting the peak of RMS to a lower capacity (Figure 6, two pulses). In comparison to the ideal rectifier scenario (Figure 5), the peak of RMS occurs at 300 µF instead of the previously observed range of 400–500 µF. However, when longer input signals are encountered, the RMS peak value shifts to higher capacities and exhibits a slightly reduced sharpness. For instance, when a 10-pulse-long rectified signal is applied to the capacitor and the load, the peak value for the RMS voltage is observed in the range of 500–600 µF, which is close to the modelled capacity peak for V_{min} (Figure 4b).

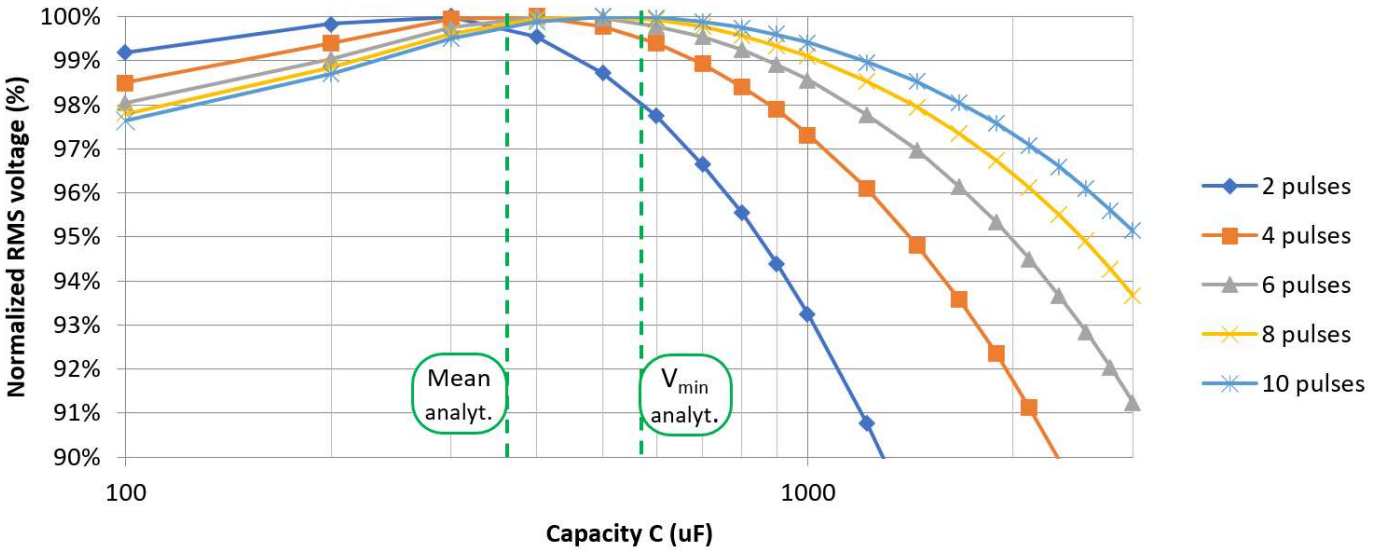

Figure 6. RMS of rectified signal with non-linear diode models at different count of rectified voltage pulses (two pulses equal one sinewave period at the input) according to the SPICE-based simulation. Each RMS value is normalized with respect to the highest value within the corresponding input signal length. Green vertical lines represent the capacity values of the mean voltage and the lowest voltage (V_{min}) peaks, as predicted by our analytical model (Figure 3d).

3.2. Experimental Validation with an Active Load and Idealized Input

3.2.1. Modelled Full-Bridge Rectifier

A typical load for energy harvesters is a voltage converter. The self-starting, low-voltage step-up converter EH4205 by Advanced Linear Devices [33] was chosen, as it has been shown before to operate with human motion energy harvesters with matching parameters [15]. The converter has an equivalent input impedance of 50 Ω, as per the modelled characteristics, and it has a 1 mF capacitor as a storage element for harvested energy. The input voltage source is a signal generator, which outputs two periods of a 20 Hz sine wave with amplitude of 800 mV and then a pause of about 530 ms to mimic an actual human motion energy harvester (Figure 1a). Internal resistance of the generator (50 Ω) is matched to the metioned harvester (19 Ω) with a resistor in parallel to the source. The full-bridge rectifier is composed of previously simulated diode model. The circuit is shown on Figure 7.

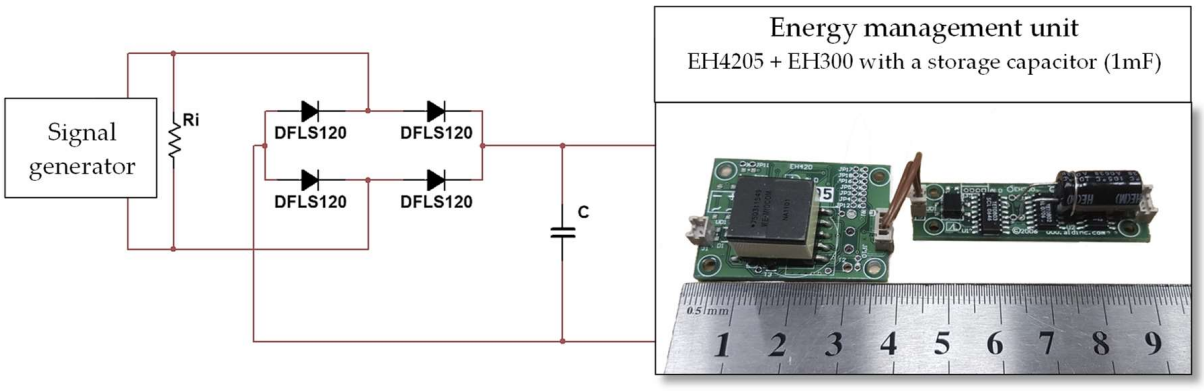

Figure 7. Circuit for experimental validation of the modelled results with a signal generator. Ri, matching resistor to create an equivalent of approximately 19 Ω; C, smoothing capacity changed during the experiment; EH4205, low-voltage step-up converter; EH300, energy storage controller.

As the low-voltage converter changes its input parameters depending on voltage on the storage capacitor [15], the experiment was timed until the same fixed value was reached on it during every measurement. Both smoothing and storage capacitors were discharged between experiments. The RMS of the rectified voltage and mean output power of the converter while charging the capacitor was evaluated (Figure 8). The rectified voltage exhibited a clear peak value at around 600 µF, which is close to the modelled peak for V_{min} (Figure 3d), while the mean output power of the converter showed its highest value in the 200–300 µF range. The reason for the difference lies in the non-linear characteristics of the used converter, and details are discussed in the Section 4. Overall, the experiment confirms the existance of the predicted smoothing capacity influence at the expected values for a circuit with active switching load.

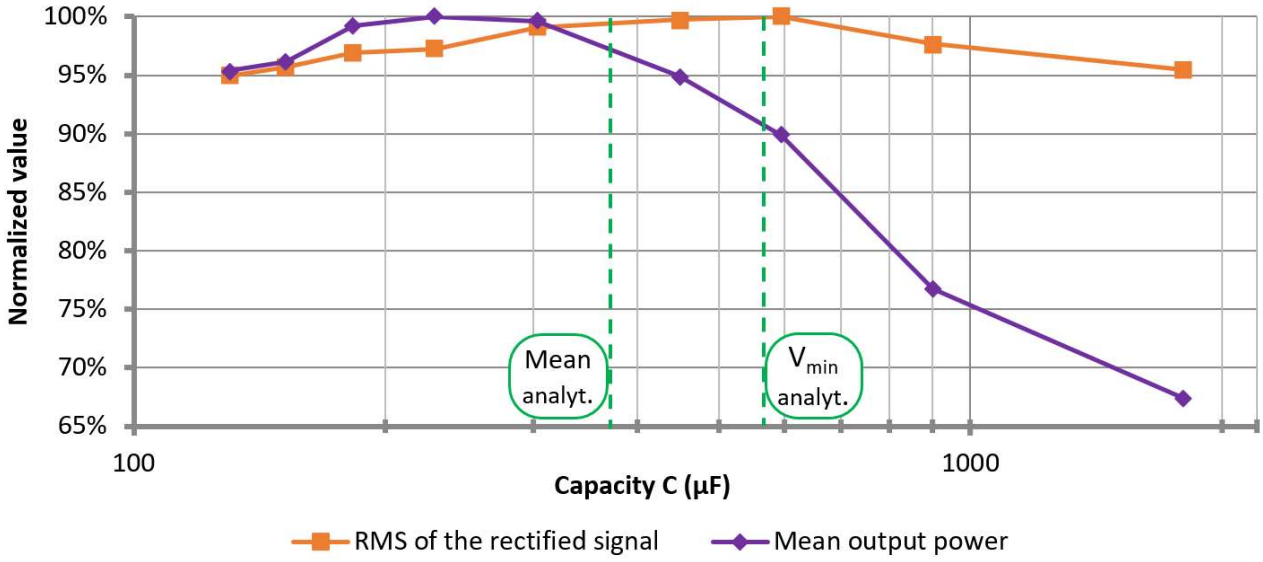

Figure 8. RMS and converter output power vs. smoothing capacity according to measurements. Values are normalized in respect to the corresponding highest value. Green vertical lines represent the capacity values of the mean voltage and the lowest voltage (V_{min}) peaks, as predicted by our analytical model (Figure 3d).

3.2.2. Simulated Voltage Doubler

The proposed model cannot be directly applied to different rectification circuits without modifications; thus, computer simulation based on SPICE models was used for a voltage doubler (Figure 9a). A pre-recorded harvester signal with the typical pauses (Figure 1a) and the same realistic diode models [32] were utilized to obtain real-life details, and a load value of 1 kΩ was used. Both capacities of the voltage multiplier were changed at the same time, and a 30 s long input signal was simulated to obtain the RMS values (Figure 9b), which show a distinct peak value in the 1.7–1.9 mF region.

Experimental validation for the voltage multiplier was conducted with a procedure matching thatas in Section 3.2.1 and with the same signal source but a different low-voltage step-up converter, with input impedance of around 1 kΩ—EH4295, by Advanced Linear Devices [34]. All capacitors were discharged between experiments. The results show a distinctive peak value for both rectified voltage and mean output power of the converter at 1.8 mF (Figure 10), which precisely aligns with the simulated result and shows very close relative values. The sesults confirm similar influencing characteristics of the capacitors between the voltage multiplier circuit and full-bridge rectifier.

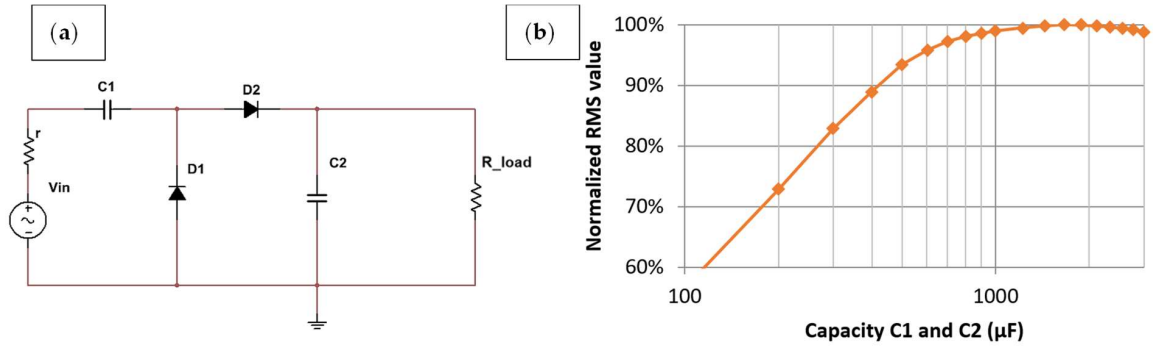

Figure 9. Simulation circuit (**a**), where both capacities C1 and C2 were changed simultaneously, $r = 19\ \Omega$, $f = 20$ Hz, $R_{load} = 1\ k\Omega$, and the normalized RMS of the rectified voltage on the load vs. capacity C1 and C2 (**b**), SPICE-based simulation.

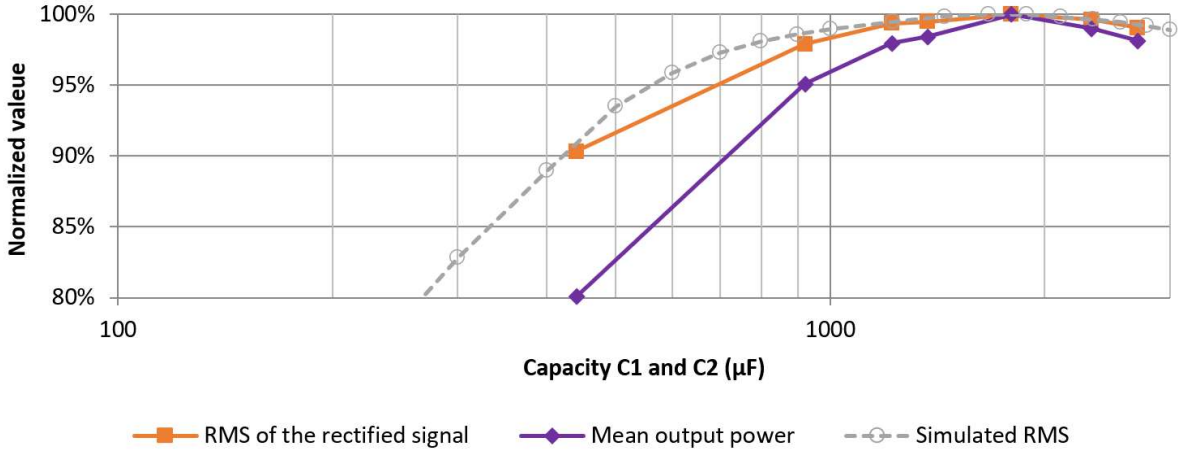

Figure 10. RMS and converter output power vs. capacity C1 and C2 in the voltage multiplier according to measurements. Values normalized in respect to highest value, simulated reference data from Figure 9b.

3.3. Experimental Validation with an Active Load and Naturally Varying Signal

A human motion energy harvester with internal resistance of 19 Ω, integrated into a man's jacket [31], was utilized in the study. This energy harvester generates power when the hand moves along the body during walking, and the participant imitated this motion while standing in place. The voltage-doubler circuit and low-voltage converter, as described in Section 3.2.2, were employed for testing. Three different capacity values were tested: 450 µF, 1800 µF, and 2700 µF. These values represent the previously tested extremes as well as the determined optimal capacity value. Each capacity was tested 10 times, and measurements were timed until the output storage capacitor reached a fixed voltage. Average values were calculated for each set of measurements, and standard deviations were estimated to evaluate the variability in the generator's performance. The results were normalized in respect to the corresponding maximum value (Figure 11).

Despite inherent variations in the generated signal, which were evident from the deviation of the results, the previously observed optimal capacity value for the highest RMS value and output power remained consistent. Increasing the capacity above 1800 µF resulted in a comparatively smaller loss in value compared to lower capacity, aligning with the previous experiment and prediction (Figures 9b and 10). However, both non-optimal values exhibited a greater relative decrease compared to the prior experiment conducted with a stable, idealized signal. That can be attributed to lower voltage due to the specific shape of the input signal (Figure 1a) and its natural variations.

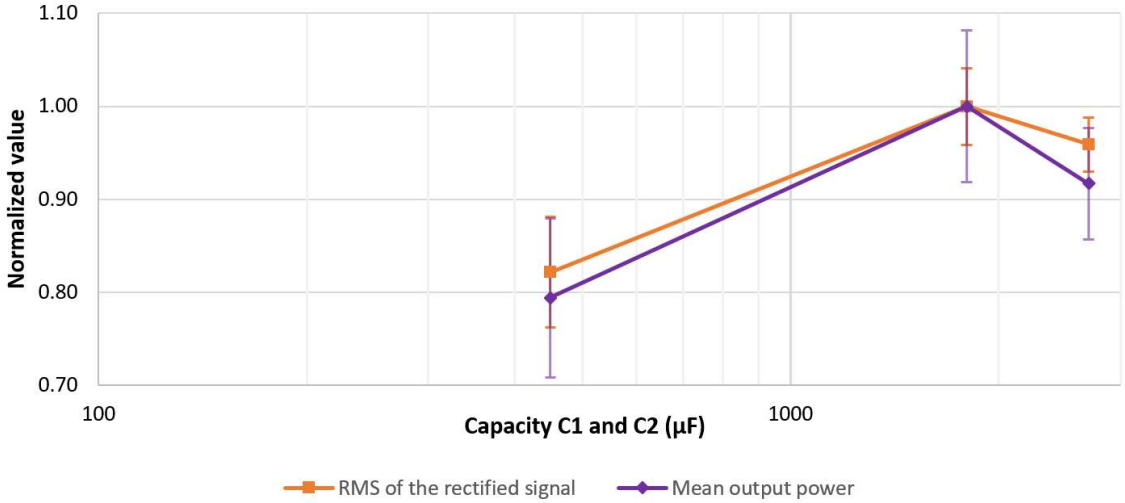

Figure 11. RMS and converter output power vs. capacity C1 and C2 in the voltage multiplier. Experimental measurements with actual human motion energy harvester; error bars represent standard deviation for each capacity measurement series.

4. Discussion

To explore the impact of smoothing capacity on the performance of a full-bridge rectifier for intermittent signals, we developed an analytical model that incorporates essential parameters like load resistance, input signal frequency, and circuit losses (e.g., internal resistance of the generator). Our model predicts that, depending on these parameters, the rectifier will deliver the highest minimal voltage V_{min} only at a specific smoothing capacity. Moreover, it enables the attainment of the highest mean value of the rectified voltage, thereby maximizing rectifier efficiency. In contrast, existing analytical models are designed for stable, uninterrupted signal rectification and predict an increase and eventual saturation of the mean rectified voltage with increasing smoothing capacity. For instance, the analytical model proposed in the work [27], when applied to the same input parameters as our model in Figure 3, demonstrates a steady increase in mean voltage and a decrease in ripple with increasing capacity (Figure 12), which is ultimately limited by losses. However, our proposed model reveals a significantly different influence for short and intermittent input signals (Figure 3d), which are more common for non-inertial mechanical energy harvesters. The proposed model and existing stationary signal models are based on mutually exclusive operating conditions and cannot be directly compared; nevertheless, this demonstrates a significant difference in the influence of smoothing capacity depending on the type of input signal. This difference may have been previously overlooked, primarily because practical applications rarely involve short, intermittent power pulses.

There are several shortcomings of the proposed model. It tends to predict lower voltage values (Figure 4) and is only applicable to static losses r, but non-linear elements like diodes change their resistance depending on the input signal, meaning their average values might need to be applied to the model. The proposed model focuses solely on predicting the voltage between the first two rectified pulses. Consequently, when a longer input signal is encountered, the displayed peak values gradually flatten out and shift towards higher capacities, as demonstrated in the simulations (Figure 6). Ultimately, the relationship between the rectified voltage and the smoothing capacity will resemble the predictions of stationary-input models, as illustrated in Figure 12. The precise number of uninterrupted input signal periods required for this transition is not covered by this study and likely relies on the circuit parameters. In our simulations, a distinct peak value was observed for up to five input periods (Figure 6). This suggests that the effect encountered at the start of the multi-period signal can persist even in a longer time span, showing its significant impact.

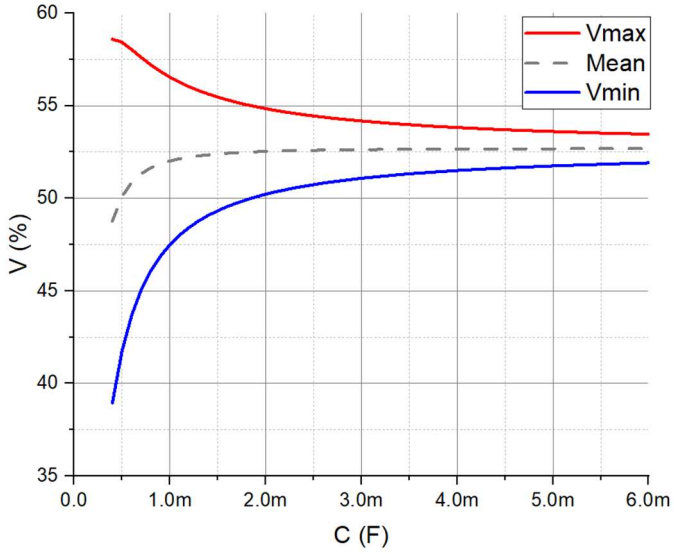

Figure 12. Rectified voltage as percentage of the input amplitude vs. smoothing capacity for a full-bridge rectifier, calculated by using a stationary input signal model by [27]; r = 19 Ω; f = 20 Hz; R_{load} = 50 Ω.

By evaluating the RMS value of the whole rectified signal, the obtained relationship indicated the peak value at the smoothing capacity between the predicted mean and the lowest voltage peak (see Figures 3d and 5). Introducing additional losses in the circuit, such as non-ideal rectification elements, and extending the length of the input signals causes this peak capacity value to shift towards either side. However, simulations consistently demonstrated and the practical experiment also confirmed (Figure 8) that the peak value predominantly remains within the capacity range defined by the predicted mean and V_{min} voltage peaks, even for an active switching load like a low-voltage converter. This suggests that the modeled results can effectively guide the selection of smoothing capacity for short, intermittent signals. Specifically, if the expected input signal spans several periods, the capacity should be chosen around the predicted V_{min} peak. Alternatively, this predicted region can serve as a guideline for experimental testing, omiting other capacity values and enabling faster identification of the most suitable capacity, for instance, in case of specific and varying input signals.

The presence of an optimal capacity for intermittent signals was further confirmed in a voltage multiplier circuit, thereby validating the existence of this relationship across various circuits where capacitors are periodically charged from zero using voltage pulses. To explore this phenomenon in circuit configurations that currently lack analytical models, computer simulations utilizing SPICE models serve as a valuable tool, offering detailed settings and providing matching results with real-life tests (Figure 10). It is worth mentioning that these simulations can be computationally intensive since they involve calculating full waveforms of the output signal before proceeding with further processing to extract the desired values. Despite the proposed full-bridge model taking certain simplifications, it has been demonstrated to yield results that closely align with the simulations. Furthermore, the graphical solution method employed by the proposed model allows for a rapid attainment of the desired outcome.

It should be noted that active loads may not always exhibit the highest performance at the maximum RMS input (as depicted in Figure 8 compared to Figure 10). Presumably, this behavior is attributed to the dependency of the converter efficiency on the input voltage (Figure 13). Specifically, in the full-bridge experiment (Section 3.2.1), the highest RMS value recorded was 95 mV, falling on the start of a steep efficiency curve (Figure 13, EH4205). Consequently, at a lower capacity value, wherein the RMS value had not yet decreased by more than 3%, but V_{max} had notably increased according to the model, and the converter was able to harness the advantages of higher peaks. This, in turn, yielded

a higher performance benefit due to the steep efficiency curve with respect to the input voltage. In contrast, the voltage-doubler experiment exhibited an RMS value as high as 470 mV, representing a more stable efficiency region on the curve (Figure 13, EH4295). Correspondingly, it exhibited the highest performance at the peak of its input RMS voltage, as illustrated in Figure 10. However, the notably higher RMS value was the result of not only the voltage multiplier but also a higher load value (1 kΩ vs. 50 Ω). This, in turn, decreased the current and subsequently reduced losses in the rectifier elements.

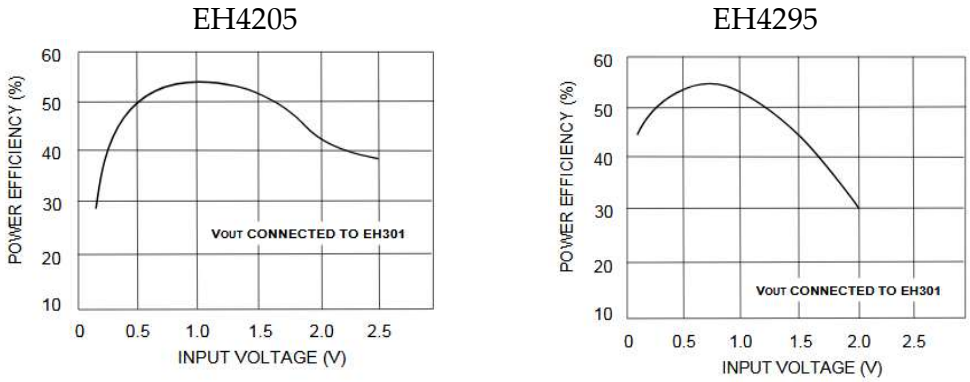

Figure 13. Power efficiency of the used low-voltage converters as a function of input voltage according to manufacturers data [33,34].

The experimentally obtained results based on an idealized input signal successfully demonstrated the modeled and simulated impact of capacity on rectifier performance (Section 3.2). However, real-life scenarios often involve variable harvester generation. To address this limitation, an experiment was conducted using an actual human motion energy harvester (Section 3.3). Repeated measurements revealed a significant variance in the RMS values, reaching up to 10.8%, representing the unstable nature of human motion. Despite this variability, the average values exhibited the expected behavior, with the highest rectified voltage RMS value aligning with the predicted capacity value. The accuracy can be attributed to the fact that the main impact of human motion variations is primarily on the amplitude of the generated signal. As described in Equations (3) and (8) of the proposed model, these variations predominantly affect the magnitude of the voltage, which explains why the capacity prediction remains consistent despite the observed variations, validating the usefulness of capacity optimization for real-life applications.

5. Conclusions

An analytical model was developed to investigate the impact of smoothing capacity on the output voltage of a full-bridge rectifier when operating with short, intermittent signals. It uses input signal frequency, load resistance, and static losses in the circuit, such as the internal resistance of the generator, to determine the trend of achievable voltage on the load based on the smoothing capacity. Notably, an optimal capacity value was identified, which leads to the highest mean voltage on the load, consequently, achieving the highest rectification efficiency. Importantly, the model can be solved graphically, reducing the computational resources otherwise required for detailed circuit simulations. Furthermore, the model showed close approximation of an optimal capacity in the case of multiple-period input signals and non-linear rectification elements.

The existence of an optimal capacity for intermittent signals was further confirmed through simulation conducted on a voltage multiplier circuit, validating that the observed relationship exists across different circuits in which capacitors are periodically charged from zero using voltage pulses. Experimental testing utilizing a generator as a source and a low-voltage step-up converter confirmed the predicted optimal capacity values for both full-bridge and multiplier circuits. Deviating from the optimal smoothing capacity resulted in a decrease in rectified RMS voltage by up to 5% for the full-bridge circuit and 10% for

the voltage multiplier circuit, which in return significantly decreased the output power of different converters by up to 33% and 20%. The real-world experiments conducted with a human motion energy harvester and voltage multiplier demonstrated an average loss of RMS voltage for non-optimal capacities of up to 15% and substantial performance degradation of the low-voltage converter by at least 20%, evidencing significant improvements of the capacity-optimized rectifier even in varying generation environments.

Author Contributions: Conceptualization, methodology, investigation, visualization, and writing—original draft preparation, I.G.; writing—review and editing, I.G. and J.B.; supervision, J.B. All authors have read and agreed to the published version of the manuscript.

Funding: This research received no external funding.

Institutional Review Board Statement: Not applicable.

Informed Consent Statement: Not applicable.

Data Availability Statement: Not applicable.

Conflicts of Interest: The authors declare no conflict of interest.

References

1. Sudevalayam, S.; Kulkarni, P. Energy Harvesting Sensor Nodes: Survey and Implications. *IEEE Commun. Surv. Tutor.* **2011**, *13*, 443–461. [CrossRef]
2. Kuang, Y.; Zhu, M. Characterisation of a knee-joint energy harvester powering a wireless communication sensing node. *Smart Mater. Struct.* **2016**, *25*, 055013. [CrossRef]
3. Gubbi, J.; Buyya, R.; Marusic, S.; Palaniswami, M. Internet of Things (IoT): A vision, architectural elements, and future directions. *Future Gener. Comput. Syst.* **2013**, *29*, 1645–1660. [CrossRef]
4. Xu, L.D.; He, W.; Li, S. Internet of Things in Industries: A Survey. *IEEE Trans. Ind. Inf.* **2014**, *10*, 2233–2243. [CrossRef]
5. Yau, C.-W.; Kwok, T.T.-O.; Lei, C.-U.; Kwok, Y.-K. Energy Harvesting in Internet of Things. In *Internet of Everything*; Di Martino, B., Li, K.-C., Yang, L.T., Esposito, A., Eds.; in Internet of Things; Springer: Singapore, 2018; pp. 35–79. [CrossRef]
6. Musiani, D.; Lin, K.; Rosing, T.S. Active Sensing Platform for Wireless Structural Health Monitoring. In Proceedings of the 2007 6th International Symposium on Information Processing in Sensor Networks, Cambridge, MA, USA, 25–27 April 2007; pp. 390–399. [CrossRef]
7. Yu, H.; Yue, Q. Indoor Light Energy Harvesting System for Energy-aware Wireless Sensor Node. *Energy Procedia* **2012**, *16*, 1027–1032. [CrossRef]
8. Khalifa, M.; Peravali, S.; Varsha, S.; Anandhan, S. Piezoelectric Energy Harvesting Using Flexible Self-Poled Electroactive Nanofabrics Based on PVDF/ZnO-Decorated SWCNT Nanocomposites. *JOM* **2022**, *74*, 3162–3171. [CrossRef]
9. Yi, F.; Lin, L.; Niu, S.; Yang, P.K.; Wang, Z.; Chen, J.; Zhou, Y.; Zi, Y.; Wang, J.; Liao, Q.; et al. Stretchable-Rubber-Based Triboelectric Nanogenerator and Its Application as Self-Powered Body Motion Sensors. *Adv. Funct. Mater.* **2015**, *25*, 3688–3696. [CrossRef]
10. Pillatsch, P.; Yeatman, E.; Holmes, A. Real World Testing of A Piezoelectric Rotational Energy Harvester For Human Motion. *J. Phys.* **2013**, *476*, 6. [CrossRef]
11. Maharjan, P.; Cho, H.; Rasel, M.S.; Salauddin, M.; Park, J.Y. A fully enclosed, 3D printed, hybridized nanogenerator with flexible flux concentrator for harvesting diverse human biomechanical energy. *Nano Energy* **2018**, *53*, 213–224. [CrossRef]
12. Mohsen, S.; Zekry, A.; Youssef, K.; Abouelatta, M. A Self-powered Wearable Wireless Sensor System Powered by a Hybrid Energy Harvester for Healthcare Applications. *Wirel. Pers. Commun.* **2021**, *116*, 3143–3164. [CrossRef]
13. Song, Y.; Min, J.; Yu, Y.; Wang, H.; Yang, Y.; Zhang, H.; Gao, W. Wireless battery-free wearable sweat sensor powered by human motion. *Sci. Adv.* **2020**, *6*, eaay9842. [CrossRef]
14. Li, Z.; Luo, J.; Xie, S.; Xin, L.; Guo, H.; Pu, H.; Yin, P.; Xu, Z.; Zhang, D.; Peng, Y.; et al. Instantaneous peak 2.1 W-level hybrid energy harvesting from human motions for self-charging battery-powered electronics. *Nano Energy* **2021**, *81*, 105629. [CrossRef]
15. Gorņevs, I.; Blūms, J.; Jurķāns, V. Performance Analysis of Low Voltage Converters for Completely Integrable Wearable Human Motion Energy Harvester. In Proceedings of the 2018 16th Biennial Baltic Electronics Conference (BEC), Tallinn, Estonia, 8–10 October 2018; pp. 1–4. [CrossRef]
16. Jurkans, V.; Blums, J.; Gornevs, I. Harvesting Electrical Power from Body Heat Using Low Voltage Step-up Converters with Thermoelectric Generators. In Proceedings of the 2018 16th Biennial Baltic Electronics Conference (BEC), Tallinn, Estonia, 8–10 October 2018; pp. 1–4. [CrossRef]
17. Hamid, R.; Yuce, M.R. A wearable energy harvester unit using piezoelectric–electromagnetic hybrid technique. *Sens. Actuators A Phys.* **2017**, *257*, 198–207. [CrossRef]
18. Bai, S.; Cui, J.; Zheng, Y.; Li, G.; Liu, T.; Liu, Y.; Hao, C.; Xue, C. Electromagnetic-triboelectric energy harvester based on vibration-to-rotation conversion for human motion energy exploitation. *Appl. Energy* **2023**, *329*, 120292. [CrossRef]

19. Luo, A.; Xu, W.; Sun, J.; Xi, K.; Tang, S.; Guo, X.; Lee, C.; Wang, F. Vibration energy harvester with double frequency-up conversion mechanism for self-powered sensing system in smart city. *Nano Energy* **2023**, *105*, 108030. [CrossRef]
20. Gorņevs, I.; Blūms, J. Investigation of Electromagnetic Harvester with Flat Structure and Low Voltage Rectifier. In Proceedings of the 10th International Conference of Young Scientists on Energy Issues (CYSENI 2013): Conference Proceedings, Kaunas, Lithuania, 29–31 May 2013; pp. 206–213.
21. Herbawi, A.S.; Velarde, F.; Paul, O.; Galchev, T. Self-powered CMOS active rectifier suitable for low-voltage mechanical energy harvesters. In Proceedings of the 2016 IEEE SENSORS, Orlando, FL, USA, 30 October–3 November 2016; pp. 1–3. [CrossRef]
22. Schade, O.H. Analysis of Rectifier Operation. *Proc. IRE* **1943**, *31*, 341–361. [CrossRef]
23. Kassakian, J.G.; Schlecht, M.F.; Verghese, G.C. *Principles of Power Electronics*; Addison-Wesley Series in Electrical Engineering; Addison-Wesley: Reading, MA, USA, 1991; p. 38.
24. Copello, M. Voltage Smoothing with a Capacitor. *Undergrad. J. Math. Model. One + Two* **2013**, *5*, 2. [CrossRef]
25. Shepherd, W.; Zhang, L. *Power Converter Circuits*; CRC Press: Boca Raton, FL, USA, 2004; p. 20.
26. Wu, K.C. *Power Rectifiers, Inverters, and Converters: Accelerated Steady-State Approaches with Closed-Form Solutions*; Lulu Press, Inc.: Morrisville, NC, USA, 2008.
27. Wu, K. Analyzing Full-Wave Rectifiers with Capacitor Filters. *Power Electron.* **2010**, *36*, 16–19.
28. Wang, C.; Lai, S.-K.; Wang, J.-M.; Feng, J.-J.; Ni, Y.-Q. An ultra-low-frequency, broadband and multi-stable tri-hybrid energy harvester for enabling the next-generation sustainable power. *Appl. Energy* **2021**, *291*, 116825. [CrossRef]
29. Wang, J.; Liang, J. Energy Harvesting from Horizontal and Vertical Backpack Movements During Walking. In Proceedings of the 2018 IEEE/ASME International Conference on Advanced Intelligent Mechatronics (AIM), Auckland, New Zealand, 9–12 July 2018; pp. 798–803. [CrossRef]
30. Lin, J.; Liu, H.; Chen, T.; Yang, Z.; Sun, L. A rotational wearable energy harvester for human motion. In Proceedings of the 2017 IEEE 17th International Conference on Nanotechnology (IEEE-NANO), Pittsburgh, PA, USA, 25–28 July 2017; pp. 22–25. [CrossRef]
31. Blums, J.; Gornevs, I.; Terlecka, G.; Jurkans, V.; Vilumsone, A. Wearable Human Motion and Heat Energy Harvesting System with Power Management. In *Energy Harvesting*; Manyala, R., Ed.; InTech: London, UK, 2018. [CrossRef]
32. Diodes Incorporated. DFLS120L—Schottky (.5A and Above). 11 January 2016. Available online: https://www.diodes.com/products/discrete/diodes-and-rectifiers/rectifiers/schottky-5a-and-above/ (accessed on 27 May 2020).
33. EH4205 Datasheet. Available online: http://aldinc.com/pdf/EH4205.pdf (accessed on 3 March 2018).
34. EH4295 Datasheet. Available online: http://aldinc.com/pdf/EH4295.pdf (accessed on 4 March 2018).